



Aalborg Universitet

AALBORG UNIVERSITY
DENMARK

Robust simultaneous myoelectric control of multiple degrees of freedom in wrist-hand prostheses by real-time neuromusculoskeletal modeling

Sartori, Massimo; Durandau, Guillaume; Došen, Strahinja; Farina, Dario

Published in:
Journal of Neural Engineering

DOI (link to publication from Publisher):
[10.1088/1741-2552/aae26b](https://doi.org/10.1088/1741-2552/aae26b)

Publication date:
2018

Document Version
Accepted author manuscript, peer reviewed version

[Link to publication from Aalborg University](#)

Citation for published version (APA):
Sartori, M., Durandau, G., Došen, S., & Farina, D. (2018). Robust simultaneous myoelectric control of multiple degrees of freedom in wrist-hand prostheses by real-time neuromusculoskeletal modeling. *Journal of Neural Engineering*, 15(6), 066026. Advance online publication. <https://doi.org/10.1088/1741-2552/aae26b>

General rights

Copyright and moral rights for the publications made accessible in the public portal are retained by the authors and/or other copyright owners and it is a condition of accessing publications that users recognise and abide by the legal requirements associated with these rights.

- Users may download and print one copy of any publication from the public portal for the purpose of private study or research.
- You may not further distribute the material or use it for any profit-making activity or commercial gain
- You may freely distribute the URL identifying the publication in the public portal -

Take down policy

If you believe that this document breaches copyright please contact us at vbn@aub.aau.dk providing details, and we will remove access to the work immediately and investigate your claim.

ACCEPTED MANUSCRIPT

Robust Simultaneous Myoelectric Control of Multiple Degrees of Freedom in Wrist-Hand Prostheses by Real-Time Neuromusculoskeletal Modeling

To cite this article before publication: Massimo Sartori *et al* 2018 *J. Neural Eng.* in press <https://doi.org/10.1088/1741-2552/aae26b>

Manuscript version: Accepted Manuscript

Accepted Manuscript is “the version of the article accepted for publication including all changes made as a result of the peer review process, and which may also include the addition to the article by IOP Publishing of a header, an article ID, a cover sheet and/or an ‘Accepted Manuscript’ watermark, but excluding any other editing, typesetting or other changes made by IOP Publishing and/or its licensors”

This Accepted Manuscript is © 2018 IOP Publishing Ltd.

During the embargo period (the 12 month period from the publication of the Version of Record of this article), the Accepted Manuscript is fully protected by copyright and cannot be reused or reposted elsewhere.

As the Version of Record of this article is going to be / has been published on a subscription basis, this Accepted Manuscript is available for reuse under a CC BY-NC-ND 3.0 licence after the 12 month embargo period.

After the embargo period, everyone is permitted to use copy and redistribute this article for non-commercial purposes only, provided that they adhere to all the terms of the licence <https://creativecommons.org/licenses/by-nc-nd/3.0>

Although reasonable endeavours have been taken to obtain all necessary permissions from third parties to include their copyrighted content within this article, their full citation and copyright line may not be present in this Accepted Manuscript version. Before using any content from this article, please refer to the Version of Record on IOPscience once published for full citation and copyright details, as permissions will likely be required. All third party content is fully copyright protected, unless specifically stated otherwise in the figure caption in the Version of Record.

View the [article online](#) for updates and enhancements.

Robust Simultaneous Myoelectric Control of Multiple Degrees of Freedom in Wrist-Hand Prostheses by Real-Time Neuromusculoskeletal Modeling

Massimo Sartori^{1,*}, Guillaume Durandau¹, Strahinja Došen², and Dario Farina³

¹Department of Biomechanical Engineering, University of Twente, NETHERLANDS

² Department of Health Science and Technology, Faculty of Medicine, Aalborg University, DENMARK

³Department of Bioengineering, Imperial College London, UNITED KINGDOM

*Address of correspondence

Massimo Sartori, Ph.D.

Assistant Professor

University of Twente

TechMed Centre

Faculty of Engineering Technology

Department of Biomechanical Engineering

Building Horsting - Room W106 - P.O. Box 217

7500 AE Enschede, The Netherlands

Email: m.sartori@utwente.nl

Keywords: electromyography; EMG-driven modeling; muscle force; musculoskeletal modeling; myoelectric prosthesis; joint moment; real-time; transradial amputee.

ABSTRACT

Objectives: Robotic prosthetic limbs promise to replace mechanical function of lost biological extremities and restore amputees' capacity of moving and interacting with the environment. Despite recent advances in biocompatible electrodes, surgical procedures, and mechatronics, the impact of current solutions is hampered by the lack of intuitive and robust man-machine interfaces. **Approach:** Based on authors' developments, this work presents a biomimetic interface that synthesizes the musculoskeletal function of an individual's phantom limb as controlled by neural surrogates, i.e. electromyography-derived neural activations. With respect to current approaches based on machine learning, our method employs explicit representations of the musculoskeletal system to reduce the space of feasible solutions in the translation of electromyograms into prosthesis control commands. Electromyograms are mapped onto mechanical forces that belong to a subspace contained within the broader operational space of an individual's musculoskeletal system. **Results:** Our results show that this constraint makes the approach applicable to real-world scenarios and robust to movement artefacts. This stems from the fact that any control command must always exist within the musculoskeletal model operational space and be therefore physiologically plausible. The approach was effective both on intact-limbed individuals and a transradial amputee displaying robust online control of multi-functional prostheses across a large repertoire of challenging tasks. **Significance:** The development and translation of man-machine interfaces that account for an individual's neuromusculoskeletal system creates unprecedented opportunities to understand how disrupted neuro-mechanical processes can be restored or replaced via biomimetic wearable assistive technologies.

53 INTRODUCTION

54 The accurate and robust decoding of human limb motor function from recordings of the underlying
55 neuromuscular activity (i.e. brain, nerve or muscle electrophysiological signals) is a complex, long-standing
56 problem [1–3]. This challenge is central for the development of control paradigms to restore lost motor
57 function in impaired individuals. Despite the advances in electromyography (EMG) and in surgical
58 procedures such as targeted muscle reinnervation [4], myoelectric prostheses still have limited clinical and
59 commercial impact [5], i.e. upper limb prostheses have peak abandonment rates between 40%-50% and
60 average rates around 25% among users [2].

61 Current myoelectric prosthesis control methods rely on machine learning where pattern recognition and
62 linear/non-linear regressions map EMGs into limb kinematics [6,7]. However, the human neuro-musculo-
63 skeletal system is characterized by multiple muscles spanning a single joint. Therefore, the same joint
64 rotation can be generated by different EMG patterns that can further vary across individuals, training
65 conditions, arm postures, or tasks [8]. The mapping functions learned in a specific condition (i.e. low force
66 tasks, or specific arm posture) do not necessarily generalize to novel conditions (i.e. high force tasks, or
67 different arm posture). Furthermore, the mapping from EMG to kinematics is not direct, as assumed in
68 machine learning schemes, i.e. limb kinematics is the musculoskeletal system final output generated by
69 series of dynamic transformations (transfer functions) in response to control commands (EMG). For this
70 reason, a single mapping function between EMGs and joint angular position (current state of the art
71 approaches) may not always capture the complexity of all intermediate nonlinear transformations [2,9].

72 A major barrier to natural artificial limb myoelectric control is the limited understanding of the
73 biomechanical and neuromuscular mechanisms governing biological joints. Here we propose an interface
74 that exploits an individual's broader neuro-mechanical information for device control rather than only the
75 underlying electrophysiological signals [1,10]. We record residual forearm EMGs from a transradial amputee
76 and intact-limbed individuals, extract EMG-based features of neural activation and concurrently drive
77 forward a subject-specific musculoskeletal model of the forearm [11–14]. This enables predicting the
78 resulting mechanical moments actuating wrist-hand joints and prescribing them in real-time to a robotic
79 multi-functional prosthesis low-level controller.

80 Although recent research demonstrated the possibility of operating EMG-driven musculoskeletal models
81 in real-time during dynamic movements [15–17], online EMG-driven modelling has never been developed

1
2 82 and applied for the control of multiple degrees of freedom (DOF) robotic limbs. To the best of our
3
4 83 knowledge the work presented in this manuscript is the first demonstration of real-time model-based
5
6 84 myoelectric prosthesis control on amputee individuals.

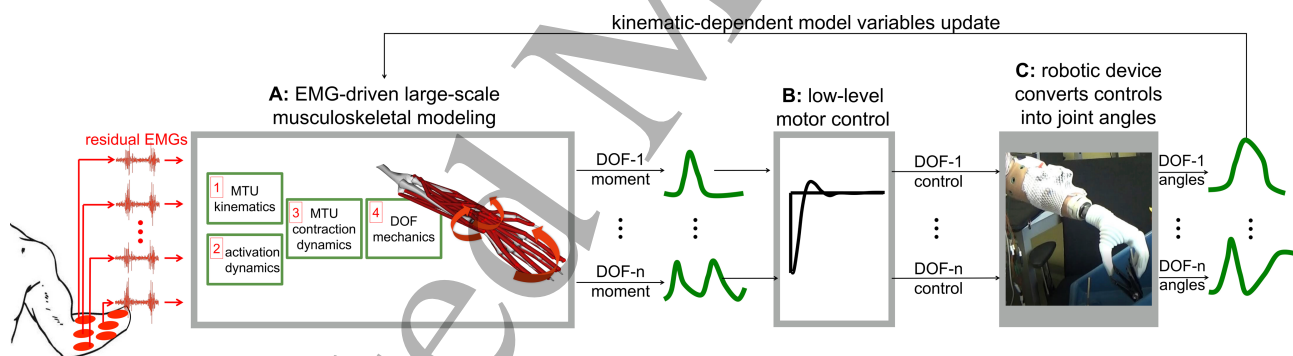
8 85 Current state of the art work proposed and tested modeling formulations in intact-limbed individuals in
9
10 86 isometric conditions and about a single joint DOF, i.e. elbow flexion-extension [18]. Although a real-time
11
12 87 two-DOF upper limb model was recently proposed [19], this was not driven by EMGs but operated via
13
14 88 simulated signals. A simplified lumped-parameter model of the hand [20,21] was recently used to compute
15
16 89 wrist and metacarpophalangeal joint flexion/extension angles in a transradial amputee. However, this did not
17
18 90 show the ability of controlling a physical prosthesis in real-time. That is, tests involved non-functional static
19
20 91 poses where the amputee controls a virtual cursor to reach given targets [20–22]. This is a major limitation.
21
22 92 Without direct proof of physical prosthesis control it is not possible to assess whether a myocontrol method
23
24 93 can be realistically employed by the user. Tests based on virtual cursor control would not account for
25
26 94 prosthesis weight, socket pressure, and prosthesis interaction with real objects, which would affect EMG
27
28 95 quality, stability, and pose a challenge for control. Tests only involving static poses would not account for
29
30 96 EMG non-stationarities (due to muscle fiber movement relative to electrode pick up areas), which may
31
32 97 further affect control performance. Moreover, these tests would not enable understanding whether reported
33
34 98 target reaching times enable prompt control of a physical prosthesis during functional tasks.

37 99 Importantly, current model-based methods integrate the dynamic equations of motions in order to predict
38
39 100 joint angles from EMGs [19,20,23]. As previously demonstrated [23], the numerical integration problem can
40
41 101 become stiff, thus displaying numerical instability in the forward dynamic simulation. As a result, due to
42
43 102 numerical integration computational load, state of the art formulations underlie simplified lumped
44
45 103 musculoskeletal models with reduced sets of DOFs, limiting translation to more proximal amputations, i.e.
46
47 104 transhumeral. These are major elements hampering robustness in the EMG-driven models currently existing,
48
49 105 which may underpin the current inability of employing EMG-driven musculoskeletal modeling for the real-
50
51 106 time control of robotic limbs.

54 107 The authors recently demonstrated the ability to establish real-time EMG-driven musculoskeletal models
55
56 108 for the online estimation of joint moments about three DOFs simultaneously in the human lower limb [24].
57
58 109 Based on this work, we here translate and embed a large-scale and physiologically-accurate EMG-driven
59
60 110 musculoskeletal model [25] into a new myoelectric control paradigm for a multifunctional robotic wrist-hand

1
2 111 prosthesis. Unlike state-of-the-art approaches, our method does not integrate the equations of motion (Fig.
3
4 112 1A). We propose a new paradigm where the physical prosthesis is used, instead of a numerical integrator
5
6 113 [20], to convert EMG-decoded joint moments into joint angles (Fig. 1B-C). Whether or not it is possible to
7
8 114 decode phantom limb joint moments, instead of joint angles, from residual muscle EMGs and concurrently
9
10 115 control a physical prosthesis represents an unanswered question. If possible, this would enable fast
11
12 116 simulation of large-scale musculoskeletal models and open up to applications requiring the control of many
13
14
15 117 DOFs, especially important for individuals who underwent targeted muscle reinnervation procedures.

16
17 118 We here show that our proposed paradigm is robust to arm postures while enabling seamless wrist-hand
18
19 119 prosthesis control across a large repertoire of functionally relevant motor tasks in an individual with
20
21 120 transradial amputation. We provide tangible results showing the successful use of a new model-based
22
23 121 paradigm in real myoelectric prosthesis control scenarios and real-world situations involving patients. The
24
25 122 novel method we propose consistently outperformed the classic two-channel control (representing the
26
27 123 commercial benchmark) in all the tests including multiple-DOF tasks as well as single-DOF tasks where the
28
29 124 commercial benchmark is expected to be best performing. To the best of our knowledge these results have
30
31 125 never been achieved by any study so far.



33
34
35
36
37
38
39
40
41
42
43 126
44
45 127 **Figure 1. Model-based control schematics for upper limb myoelectric robotic limbs.** (A) A large-scale,
46
47 128 physiologically correct musculoskeletal model predicts muscle forces of residual forearm muscles as well the
48
49 129 resulting joint moments acting on the amputee's phantom limb. (B) Joint moment estimates are converted
50
51 130 into prosthesis low-level motor commands. (C) The prosthesis is the physical device that converts EMG-
52
53
54 131 predicted joint forces into joint kinematics, rather than using numerical integration as previously 132 proposed.
55
56 This enables real-time simultaneous and proportional control multi of multiple degrees of 133 freedom (DOFs) in
57
58 myoelectric robotic limbs.

METHODS

We developed a subject-specific modeling formulation (Figs 1-2) that enabled estimation of wrist-hand musculoskeletal function in both intact-limbed individuals and transradial amputees as controlled by EMG-derived neural activations. We demonstrated the ability of using resulting model-based joint moment estimates for the concurrent, real-time control of a myoelectric prosthesis throughout a large repertoire of wrist-hand tasks. Our proposed framework schematic is depicted in Figs 1-2 and comprises three major components including: EMG-driven musculoskeletal model (Fig. 1A), prosthesis low-level controller (Fig. 1B-C), and model calibration (Fig. 2). The EMG-driven musculoskeletal model component is developed based on previous work from the authors [13–15,26–30] as well as from other groups [31–37].

Experimental procedures were performed for each individual subject on two consecutive days. During the first day, a musculoskeletal model was scaled and calibrated to match each individual's anthropometry and force-generating capacity. During the second day, the subject-specific model was employed for the online prosthesis control tests across arm configurations. Online control tests were performed with no model re-calibration and involved direct comparison with the classic two-channel control benchmark. The commercial benchmark was chosen because it provides highest robustness in the control of single-DOFs across arm configurations and therefore represents the best means for comparison with respect to our proposed method.

First, we describe how motion data were collected and processed for establishing subject-specific musculoskeletal models, i.e. see Data Recording and Processing Section. Second, we describe our proposed model-based framework components (see EMG-driven Musculoskeletal Model, Prosthesis Low-Level Controller and Model Calibration Sections) along with the communication framework that enabled data flow between EMG amplifier, prosthetic limb and model-based framework (see System Communication Framework Section). Third we describe the online prosthesis control testing procedures (see Experimental Tests Section).

Data Recording and Processing

Motion capture data were recorded (256Hz) using a seven-camera system (Qualisys, Göteborg, Sweden, 256Hz) and a set of 18 retro-reflective markers placed on the individual's intact left upper extremity, residual right upper extremity, trunk, and pelvis. Data were recorded during one static anatomical pose and used in

1
 2 164 conjunction with the open-source software OpenSim [38] to scale a generic upper extremity model of the
 3
 4 165 musculoskeletal geometry [25,39] to match the subject's anthropometry. The musculoskeletal geometry
 5
 6 166 model had six upper extremity DOFs including: shoulder elevation, shoulder adduction-abduction, elbow
 7
 8 167 flexion-extension, forearm pronation-supination, wrist flexion-extension, and first-to-fourth proximal
 9
 10 168 metacarpophalangeal joint flexion-extension. Although the model encompasses all DOFs and muscle-tendon
 11
 12 169 units (MTUs) in the human hand [25], only a subset of these were employed. Specifically, this incorporated a
 13
 14 170 total of 12 MTUs spanning the elbow, wrist and hand joints (Table I). During the scaling process, virtual
 15
 16 171 markers were placed on the generic musculoskeletal geometry model based on the position of the
 17
 18 172 experimental markers from the static pose. The model anthropomorphic properties as well as MTU insertion,
 19
 20 173 origin and MTU-to-bone wrapping points were linearly scaled on the basis of the relative distances between
 21
 22 174 experimental and corresponding virtual markers[38].

25 175 EMGs were measured (10KHz) and A/D converted with 12-bit precision using a 256-channel EMG
 26
 27 176 amplifier (OTBioelettronica, Torino, IT). Only eight channels were used for the experiment, i.e. via eight
 28
 29 177 pairs of disposable bipolar electrodes (Ambu, Neuroline 720, DK). Electrodes were placed in the
 30
 31 178 correspondence of eight upper limb muscle groups including: biceps brachii, pronator teres, extensor carpi
 32
 33 179 radialis, extensor carpi ulnaris, extensor digitorum, flexor carpi radialis, flexor carpi ulnaris, flexor
 34
 35 180 digitorum. Placement was performed following SENIAM recommendations with a 10mm inter-electrode
 36
 37 181 distance (measured from each electrode center) [40]. Each individual was initially asked to perform maximal
 38
 39 182 voluntary contractions articulating wrist flexion-extension, forearm pronation-supination, and hand opening-
 40
 41 183 closing. EMGs were high-pass filtered (30Hz), full-wave rectified, and low-pass filtered (6 Hz) using a
 42
 43 184 second-order Butterworth filter. Resulting peak-processed values were used for the subsequent EMG
 44
 45 185 normalization during the real-time myocontrol experimental tests. All tests were performed using a powered
 46
 47 186 multi-functional wrist hand prosthesis (Michelangelo Hand, Ottobock HealthCare GmbH, Duderstadt, DE)
 48
 49 187 equipped with wrist pronation-supination (WPS), flexion-extension (WFE) and hand opening-closing (HOC)
 50
 51 188 motors. The prosthesis can produce two grasp types; the palmar grasp was used (HOC) in the present study.
 52
 53 189 The hand is sensorized with embedded position and force sensors, measuring aperture size, wrist rotation
 54
 55 190 angle and grasping force. The commands to the hand and sensor data from the hand were transmitted through
 56
 57 191 a Bluetooth or TCP/IP connection (100 Hz).

192 **Table I. EMG to MTU mapping.** Mapping between experimental electromyograms (EMGs) and

1
2 193 simulated musculotendon units (MTUs)*.

3	EMGs	Biceps	Pronator	Extensor	Extensor	Extensor	Flexor	Flexor	Flexor
4		Brachii	Teres	Carp	Carp	Digitorum	Carp	Carp	Digitorum
5				Radialis	Ulnaris		Radialis	Ulnaris	
6	MTUs	BIClong,	PT,	ECRL,	ECU	EDC	FCR	FCU	FDS,
7		BICshort	PQ	ECRB					FDPM
8									

9 194 * Musculotendon unit names: biceps brachii long head (BIClong) and short head (BICshort), extensor carpi
10 195 radialis longus (ECRL), extensor carpi radialis brevis (ECRB), extensor carpi ulnaris (ECU), extensor
11 196 digitorum communis (EDC), flexor carpi radialis (FCR), flexor carpi ulnaris (FCU), flexor digitorum
12 197 superficialis (FDS), flexor digitorum profundus (FDPM), pronator quadratus (PQ), and pronator teres (PT).
13 198
14

15 199 **EMG-driven Musculoskeletal Model**

16
17 200 Our proposed EMG-driven modeling framework (Fig. 1) receives as an input: (1) EMGs from the amputee's
18
19 201 residual limb and (2) prosthesis joint angles. This information is used to compute the mechanical moments
20
21 202 produced to actuate the amputee's phantom limb and the intact-limbed individuals' wrist-hand. The EMG-
22
23 203 driven musculoskeletal modeling formulation comprises four main components [13,26,27,41]. The **neural**
24
25 204 **activation component** (Fig. 1A.1) converts EMGs into MTU-specific activation using a second order
26
27 205 muscle twitch model and a non-linear transfer function [13,30,41]. Eight EMG channels were mapped into
28
29 206 12 MTUs as detailed in Table I. The **MTU kinematics component** (Fig. 2A.2) synthesizes the MTU paths
30
31 207 defined in the subject-specific geometry model into a set of MTU-specific multidimensional cubic B-splines.
32
33 208 Each B-spline computes MTU kinematics (i.e. MTU length and moment arms) as a function of input
34
35 209 prosthesis joint angles [27]. The **MTU dynamics component** (Fig. 2A.3) solves for the dynamic equilibrium
36
37 210 between muscle fibers and series tendons in the production of MTU force. It employs a Hill-type muscle
38
39 211 model with activation-force-length-velocity relationships informed by MTU length and neural activations
40
41 212 from the previous two components [13,42]. The **joint mechanics component** (Fig. 1A.4) transfers MTU
42
43 213 forces to the skeletal joint level using MTU moment arms. This enables computing joint moments [13].
44
45 214 Unlike state of the art methods, this procedure does not require forward integration of the equations of
46
47 215 motion and is done in real-time using a physiologically correct large-scale musculoskeletal model, i.e. no
48
49 216 need for simplification in the underlying musculoskeletal structure being modeled [11].
50
51 217
52
53 218

54 218 **Prosthesis Low-Level Controller**

55 219 The joint moments predicted by the EMG-driven model are subsequently converted into prosthesis low-level
56
57 220 control commands (Fig. 1B). These are first amplitude-normalized, threshold-processed, and prescribed to
58
59
60

the prosthesis DOFs individually (Fig. 1C). The prosthesis embedded low-level controller receives input commands and rotates the prosthesis joints with a velocity profile that is proportional to the decoded joint moment. The prosthesis DOF angular kinematics is directly modulated as a function of the input command amplitude. The prosthesis movement emerging from these commands is fed into the EMG-driven model MTU kinematic component (Fig. 1A.2) and used to update the kinematic-dependent state in the musculoskeletal model. This includes skeletal DOF angular position as well as DOF-angle-dependent MTU length, MTU-to-bone wrapping points, and MTU moment arms.

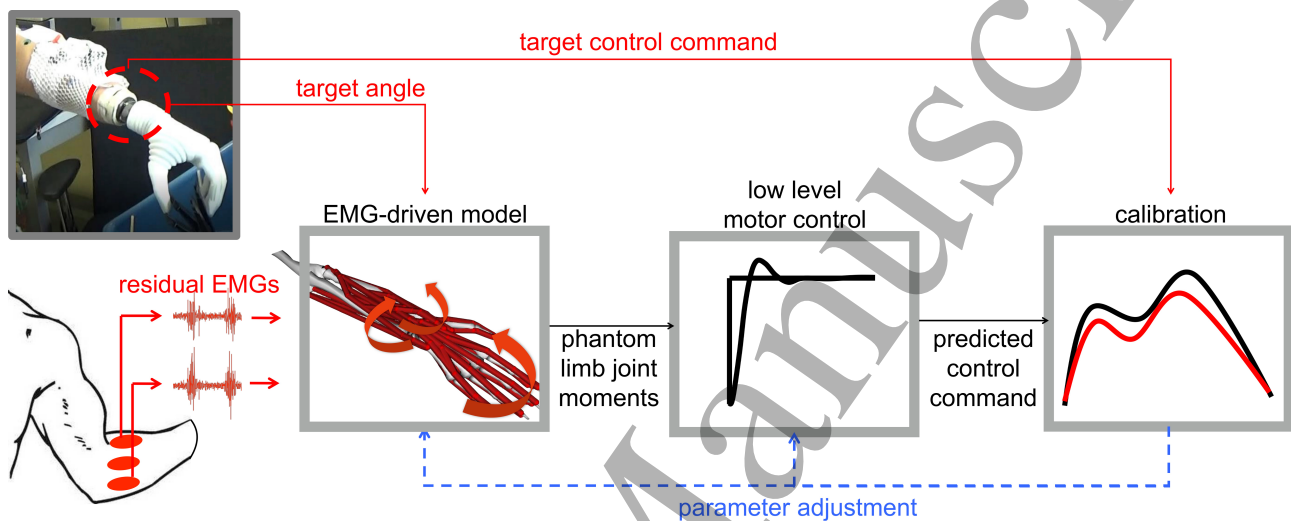


Figure 2. Model calibration procedure. The real-time EMG-driven model-based controller is calibrated using prosthesis joint motor control commands. During calibration the amputee is instructed to mimic pre-defined motions executed by the prostheses using their own phantom limb. EMG-driven model internal parameters are repeatedly refined, as part of a least-squares optimization procedure, so that the mismatch between EMG-driven model's predicted prosthesis DOF commands and those produced by the prosthesis pre-defined command inputs is minimized.

Model Calibration

During calibration, the amputee is instructed to activate the muscles in the residual limb mimicking pre-defined motions executed by the prostheses using their own phantom limb (Fig. 2). Pre-defined prostheses motions to mimic involve moving through the full range of motion about each selected DOF at a constant speed. Pre-defined motions included: wrist flexion-extension, forearm pronation-supination, and hand opening-closing. During this, the calibration algorithm receives three input signals: EMGs from the amputee's residual limb, prosthesis DOF angles, as well as the prosthesis DOF control commands

1
 2 243 (normalized velocities) producing the target DOF angles. The **calibration component** (Fig. 2) identifies a
 3
 4 244 number of amputee-specific musculoskeletal parameters that vary non-linearly across individuals because of
 5
 6 245 anatomical and physiological differences. These include: muscle twitch activation/deactivation time
 7
 8 246 constants, EMG-to-activation non-linearity factor, muscle optimal fiber length, tendon slack length, and
 9
 10 247 muscle maximal isometric force. The initial nominal parameters are repeatedly refined, as part of a least-
 11
 12 248 squares optimization procedure, so that the mismatch between EMG-driven model's predicted prosthesis
 13
 14 249 DOF commands and those applied to the prosthesis (predefined normalized velocities) is minimized.
 15
 16 250 Calibration operates offline using prerecorded data. This enables calibration of both uni-lateral and bi-lateral
 17
 18
 19 251 amputees, since the subject mirrors the movement of the prosthesis with the phantom limb (instead of
 20
 21 252 mirroring the contralateral healthy limb as in [20]).
 22

23 253

24

25 254

26

27 255

28

29 256

30

31 257

32

33 258

34

35 259

36

37 260

38

39 261

40

41 262

42

43 263

44

45 264

46

47

48

49

50

51

52

53

54 265

55 266

56

57 267

58

59 268

60

System Communication Framework

The whole real-time modeling framework (i.e. EMG-driven Model and Calibration, Figs 1-2) operated on a laptop with dual-core processing unit (2.60GHz) and 16GB of RAM memory. Based on our recent work [24] we developed two software plug-in modules that enabled direct TCP/IP connection between the real-time modeling framework and external devices. The first plug-in module provided a direct TCP/IP connection to the external EMG amplifier. It recorded the raw EMGs and processed them as described in the Data Recording and Processing Section. The second plug-in module enabled a direct TCP/IP connection to the prosthetic limb. It processed the EMG-driven model-based estimates of wrist-hand moments to produce prosthesis low-level control commands, i.e. see Prosthesis Low-Level Controller Section.

Table II. Description of subjects investigated. Intact-limbed subjects are labeled as IL1-3. The transradial amputee individual is labeled as TR1.

	Age (Years)	Weight (Kg)	Height (cm)	Sex	Number of electrodes used	Amputation Level	Years since amputation	Prosthesis use
IL1	34	68	183	Male	8	-	-	-
IL2	26	73	177	Male	8	-	-	-
IL3	40	73	176	Male	8	-	-	-
TR1	50	75	168	Male	8	Transradial	30	Daily

Experimental Tests

Experiments were conducted in accordance with the declaration of Helsinki. The University Medical Center Göttingen Ethical Committee approved all experimental procedures (Ethikkommission der

Universitätsmedizin Göttingen, approval number 22/4/16). Three intact-limbed individuals (IL1-3) and one transradial amputee (TR1, Table II) volunteered for this investigation after providing signed informed consent form. Amputation in the TR1 individual was a result of a traumatic injury at year 20th (Table II). Residual stump was estimated to be of 15 cm as measured from the stump most distal point to elbow lateral epicondyle. The TR1 individual is a regular prosthetic user currently fitted with a myocontrolled prosthesis (Michelangelo Hand, OttoBock HealthCare, GmbH) and the two-EMG-channel direct control scheme also used in our tests. None of the subjects had any neuromuscular disorder or abnormality than listed. Subjects performed three series of tasks including: virtual target reaching, clothespin, and functional tests. All tests were performed with no force feedback provided to the amputee.

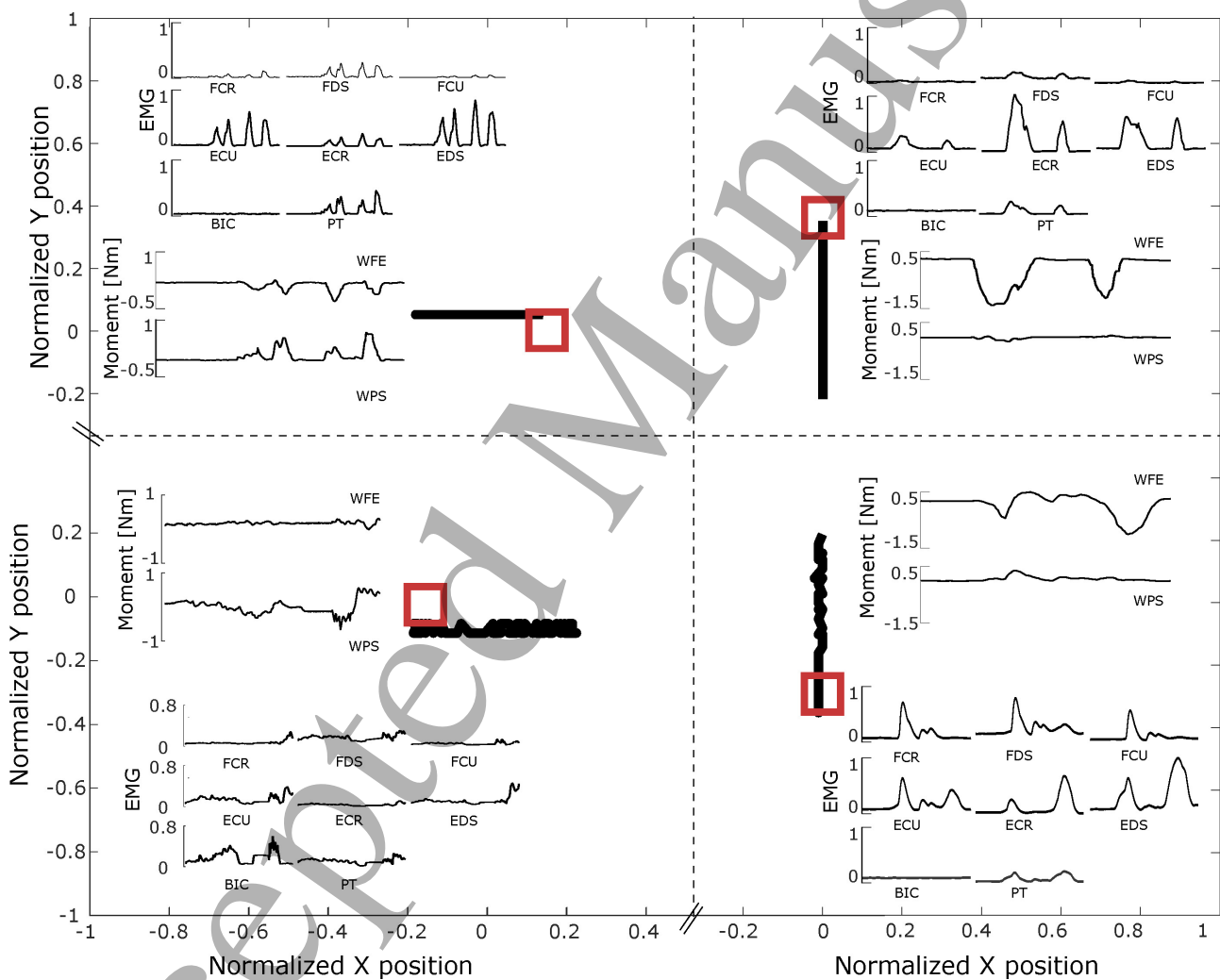
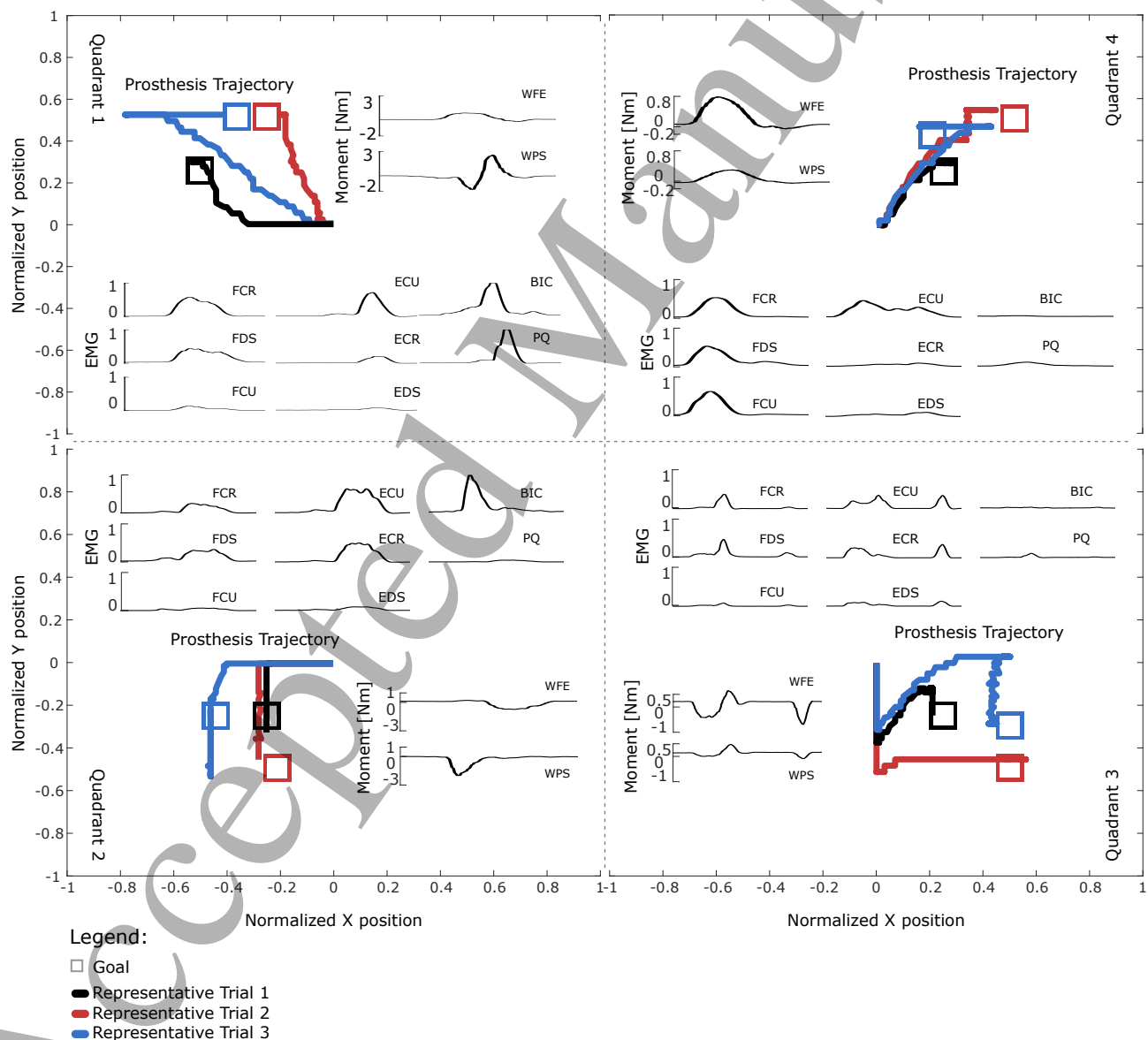


Figure 3. Vertical and horizontal target reaching tests reported for the transradial amputee (TR1).

Four representative target positions to reach are depicted as red square-shaped cursors. The target workspace spanned the interval $[-1, 1]$ in normalized units in both vertical and horizontal directions, where -1 and 1 corresponded to full pronation/flexion and supination/extension of the prosthesis. Vertical targets are

1
 2 283 accomplished by operating the prosthesis wrist flexion-extension (WFE) degree of freedom (DOF).
 3
 4 284 Horizontal targets are accomplished by operating prosthesis forearm pronation-supination (WPS) DOF. Each
 5
 6 285 target is represented along with the underlying electromyograms (EMGs) recorded from the residual forearm
 7
 8 286 muscles including: flexor/extensor carpi radialis (FCR/ECR), flexor/extensor carpi ulnaris (FCU/ECU),
 9
 10 287 flexor/extensor digitorum superficialis (FDS/EDS), pronator teres (PT), and biceps brachii (BIC).
 11
 12 288 Furthermore, the resulting DOF moments predicted at the phantom limb WFE and WPS DOFs are depicted,
 13
 14 289 i.e. see black curves in each quadrant. EMGs are depicted as dimensionless curves whereas moments are
 15
 16 290 represented in Nm.
 17
 18
 19 291
 20
 21 292
 22



60

1
2 294 **Figure 4. Diagonal target reaching tests reported for the transradial amputee (TR1).** Results are
3
4 295 reported for each of the four quadrants. See Movie 1 for a visual example of quadrant 3 reaching tasks. Three
5
6 296 representative targets per quadrant are depicted as square-shaped cursors. Each target is reached from the
7
8 297 same initial position, i.e. zero degrees of wrist flexion and forearm pronation (hand neutral position). The
9
10 298 target workspace spanned the interval $[-1, 1]$ in normalized units in vertical and horizontal directions, where
11
12 299 -1 and 1 corresponded to full pronation/flexion and supination/extension of the prosthesis. Each target is
13
14 300 reached by the simultaneous control of two degrees of freedoms (DOFs). In each quadrant, each target is
15
16 301 represented along with the underlying electromyograms (EMGs) recorded from the residual forearm muscles
17
18 302 including: flexor/extensor carpi radialis (FCR/ECR), flexor/extensor carpi ulnaris (FCU/ECU),
19
20 303 flexor/extensor digitorum superficialis (FDS/EDS), pronator teres (PT), and biceps brachii (BIC).
21
22 304 Furthermore, the resulting DOF moments predicted at the phantom limb wrist flexion-extension (WFE) and
23
24 305 forearm pronation-supination (WPS) DOFs are depicted, i.e. see black curves in each quadrant. Across all
25
26 306 quadrants and targets, vertical and horizontal directions are achieved by controlling WFE and WPS
27
28 307 respectively. EMGs are depicted as dimensionless curves whereas moments (torques) are represented in Nm.
29
30 308

31 309 **Virtual Target Reaching Tasks**

32
33 310 During the **virtual target reaching tasks**, subjects sat in front of a monitor and were asked to position
34
35 311 themselves on the chair so that their right arm could move freely in any direction. The monitor provided
36
37 312 visual feedback in the form of a ball-shaped cursor representing the prosthesis wrist flexion-extension and
38
39 313 pronation-supination kinematics state. Subjects were instructed to move a ball-shaped cursor to reach a
40
41 314 square-shaped target while keeping the cursor within the target for more than 1 second. Both cursor and
42
43 315 target moved in a Cartesian space. Cursor vertical movements were accomplished by actuating the prosthesis
44
45 316 wrist flexion-extension DOF via appropriate muscle contractions. Flexion and extension moved the cursor in
46
47 317 the negative and positive vertical directions respectively. Similarly, cursor horizontal movements were
48
49 318 accomplished by actuating the prosthesis wrist pronation-supination DOF. Pronation and supinations moved
50
51 319 the cursor in the negative and positive horizontal directions respectively. Prosthesis neutral position
52
53 320 corresponded to the cursor being in the Cartesian space origin. During all tasks, the myoelectric prosthesis
54
55 321 was located next to the subject.
56
57
58
59
60

1
2 322 The workspace spanned the interval $[-1, 1]$ in normalized units in vertical and horizontal directions,
3
4 323 where -1 and 1 corresponded to full pronation/flexion and supination/extension of the prosthesis. The
5
6 324 prosthesis wrist range of motion was $[-150, 150]$ and $[-75, 50]$ degrees for pronation/supination and
7
8 325 flexion/extension respectively. Tasks were conducted with variable travel distance that ranged between 0.35
9
10 326 and 0.7 normalized units and with constant target size of 0.2 by 0.2 normalized units. The targets were
11
12 327 centered at the coordinates $(\pm 0.25, \pm 0.25)$, $(\pm 0.25, \pm 0.5)$, $(\pm 0.5, \pm 0.25)$, and $(\pm 0.5, \pm 0.5)$, where the signs of
13
14 328 the coordinates were determined by the quadrant that was tested. Subject performed two series of tests.

15
16
17 329 The first test series verified the system robustness to hand movement artefacts. Subjects were required to
18
19 330 repeatedly open and close their right biological or phantom hands in time to an acoustic metronomic cue, i.e.
20
21 331 50 beats per seconds, 10 repeated hand opening and closings. The subjects were instructed to exert 10% of
22
23 332 their maximum opening\closing force.

24
25 333 The second test series verified the system ability to enable controlling WFE and WPS individually,
26
27 334 sequentially, as well as simultaneously. Subjects were required to perform a number of reaching tests. Each
28
29 335 test required reaching eight targets randomly located on the:

- 30
31 336 • Vertical axis only, i.e. prosthesis WFE DOF myoelectric control.
- 32
33 337 • Horizontal axis only, i.e. prosthesis WPS DOF myoelectric control.
- 34
35 338 • Cartesian space four quadrants using sequential control of prosthesis WFE and WPS DOFs.
- 36
37 339 • Cartesian space four quadrants respectively, i.e. top-left, bottom-left, top-right, bottom-right. Each
38
39 340 quadrant required the simultaneous and proportional control of the prosthesis WFE and WPS DOFs.

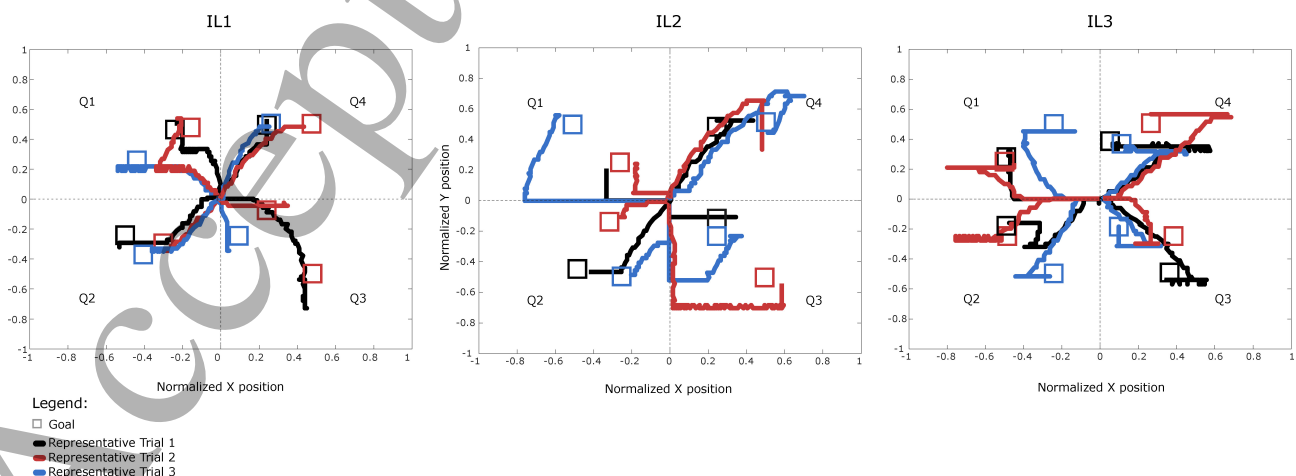
40
41
42 341 Importantly, in all the tests, the subjects could activate the DOFs simultaneously, but during horizontal,
43
44 342 vertical and sequential task, they were instructed to use a single DOF at a time. The aim of these tests was to
45
46 343 assess the selectivity of control and the amount of cross talk between the command signals (unwanted
47
48 344 activation). Each test series was repeated with the right arm in three different postures including: fully
49
50 345 extended elbow, 90 degree flexed elbow, 90 degree flexed elbow and 90 degree abducted shoulder. Arm
51
52 346 postures were monitored via inertial measurement units (XSens, Enschede, Netherlands) placed in the
53
54 347 correspondence of anatomical landmarks including: right acromion, humerus lateral compartment, forearm
55
56 348 lateral compartment. Moreover, each test was performed both using our proposed model-based system as
57
58
59
60

well as the classic commercial control system. The aim was to compare the performance of the novel method to that of the commercial benchmark.

Clothespin Task

During the **clothespin task** subjects wore the prosthesis, which was connected to their forearms. For the able-bodied subjects, the prosthesis was connected to a custom-made splint, which was then strapped to the forearm. For the amputee subject, the prosthesis was mounted to a custom-made socket (as in a real-life application). They stood in front of a clothespin test preparation platform. These tasks verified the ability to accurately control WPS and HOC simultaneously and proportionally during functionally relevant tasks. Each test was performed both using our proposed model-based system as well as the classic commercial control system. Subjects performed two series of tests. The first test series involved grasping 12 pins located on horizontal bars and placing them onto a vertical bar. Each pin triplet underlay different stiffness, hence the need for grips with different force levels. This test was designed so that the subject needed to activate WPS as well as HOC proportionally (to modulate force) and simultaneously (to activate multiple DOFs).

The second test series was a variation of the first. It involved performing a clothespin task with pins equipped with custom-made contact sensor and an LED. When the pin fully closed, the sensor activated the LED indicating that the exerted grasping force was too high, thereby “breaking” the “object”. The goal is to grasp five pins each of which of different stiffness while accurately fine-tuning the grip force in order to always keep it below a predefined threshold. More specifically, the subjects needed to exert enough force to open the pin and remove it from the bar, but at the same time, the force had to be below the “breaking” threshold of the pin. Therefore, each pin corresponded to a target window of grasping force.



1
2 371 **Figure 5. Diagonal target reaching tests reported for three intact-limbed individuals (IL1-3).** Three
3
4 372 representative targets per quadrant (Q1-Q4) are depicted as square-shaped cursors. Each target is reached
5
6 373 from the same initial position, i.e. zero degrees of wrist flexion and forearm pronation (hand neutral
7
8 374 position). The target workspace spanned the interval $[-1, 1]$ in normalized units in vertical and horizontal
9
10 375 directions, where -1 and 1 corresponded to full pronation/flexion and supination/extension of the prosthesis.
11
12 376 Each target is reached by the simultaneous control of two degrees of freedoms (DOFs). Across all quadrants
13
14 377 and targets, vertical and horizontal directions are achieved by controlling WFE and WPS respectively. Also
15
16
17 378 see Movie 1 for a visual example of Q3 reaching tasks.

18
19 379

20 21 380 **Functional Tasks**

22
23 381 During the **functional tasks**, each subject wore the prosthesis and stood in front of a shelf. These tasks
24
25 382 verified the system ability of performing real-world functions robustly and intuitively. The tasks were
26
27 383 performed solely by using our proposed model-based system. Subjects performed three testing series. The
28
29 384 first was a block-turn task [43] involving a sequence of fine control actions including: grasping a narrow
30
31 385 wooden block placed on a high self, rotating it of 90 degrees, placing it back on the shelf, re-grasping the
32
33 386 block, rotating it back of 90 degrees, and replacing the block back to its initial position.

34
35
36 387 The second involved grasping a variety of objects ranging from small size and weight to large size and
37
38 388 weight: including an egg and a big bottle (1.5L). This investigated the system robustness in handling heavy
39
40 389 objects or preserving precise grip forces while handling delicate objects (i.e. eggs).

41
42 390 The third assessed the robustness of the system to EMG movement artefacts. It involved mechanical
43
44 391 perturbation in the EMG wired system to induce cable movement. This assessed whether the prosthesis
45
46 392 would be inadvertently activated (by movement-induced noise) and whether the user could still actively
47
48 393 control the prosthesis during the high noise condition.

49
50
51
52
53
54
55
56
57
58
59
60

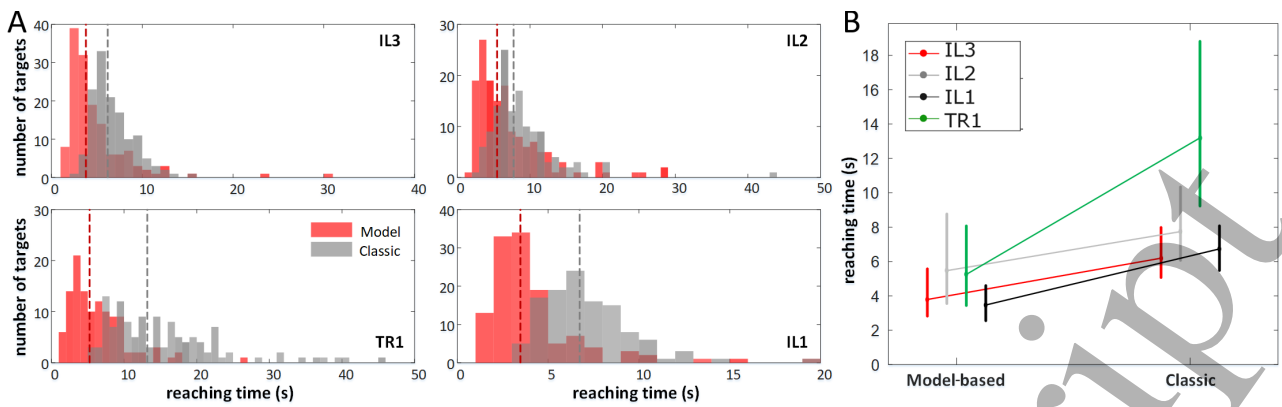


Figure 6. Speed performance during diagonal target reaching test reported for the transradial amputee (TR1) and for the three intact-limbed individuals (IL1-3). (A) Histograms report the distribution of reaching time across all targets for each subject individually, i.e. TR1 and IL1-3. Vertical dotted lines represent median reaching time. (B) Graphs report median (ball marker) and interquartile range (vertical line) of the time took to reach all targets as reported on a subject-specific basis. Targets in each quadrant and condition were accomplished both using our proposed model-based approach (model) as well as the classic commercially available system (classic).

Numerical Analysis

We quantified our proposed model-based framework real-time computation performance using metrics including: the mean computation time, standard deviation, median and 1st-3rd interquartile range measured across all simulation frames from all subjects and tasks. The 90% confidence interval was estimated for our proposed framework computation time using the Chebyshev's theorem, i.e., expected interval = mean \pm 3.16·std. This could be applied with no assumption on the normality of computation time distributions. Path similarity between reaching trajectory and shortest path was calculated using the coefficient of determination (R^2 , square of the Pearson product moment correlation coefficient). In all the reaching tasks, we have determined the mean and standard deviation for the time to reach the target. The outcome measure in the clothespin task was the number of pins transferred per minute.

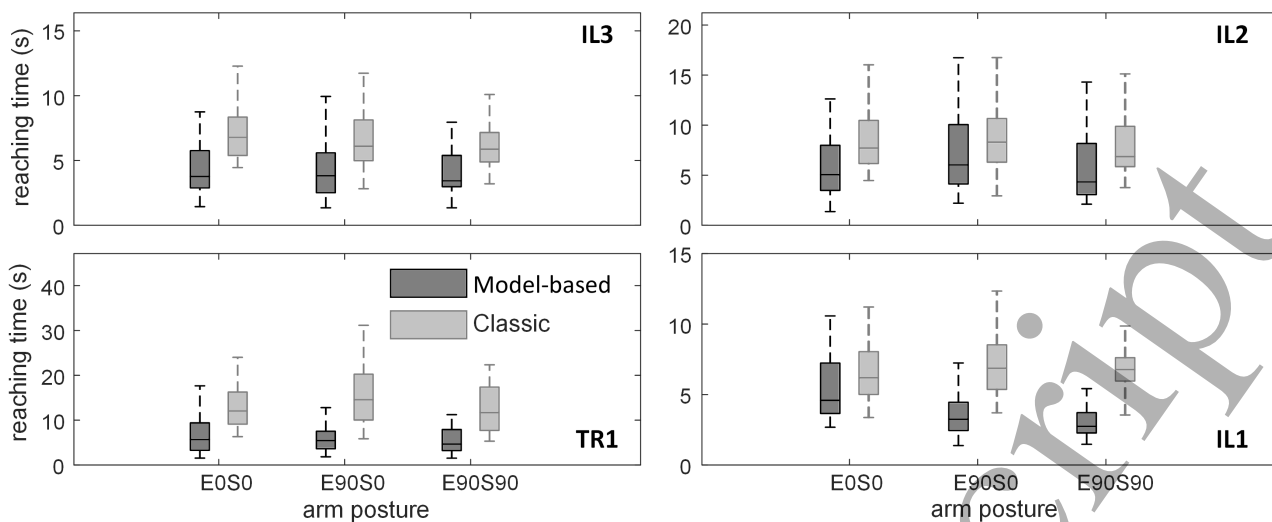


Figure 7. Speed performance as a function of arm position reported for the transradial amputee (TR1) and for the three intact-limbed individuals (IL1-3). Graphs report median (horizontal line), interquartile range (box), and overall max/min values (vertical dotted lines) of the time took to reach diagonal targets as a function of arm configurations: elbow/shoulder 0 degrees (E0S0)), elbow 90 degrees flexed, shoulder 0 degrees (E90S0), elbow 90 degrees flexed, shoulder 90 deg abducted with hand closed (E90S90). Targets in each quadrant and condition were accomplished both using our proposed model-based approach (model-based) as well as the classic commercially available system (classic).

RESULTS

Our proposed real-time musculoskeletal model successfully converted EMG signals from eight forearm muscle groups into mechanical forces produced by 12 musculotendon units or MTUs (Table I) and into resulting EMG-dependent joint moments across a large repertoire of wrist-hand movement (Fig. 1A). EMG-driven model-based joint moment estimates were translated into prosthesis control commands (Fig. 1B), which resulted in the prosthesis moving naturally with no need for explicit angular position control. The prosthesis movement emerging from these commands was directly used to update the kinematic-dependent state in the musculoskeletal model (Fig 1C).

Results showed that our proposed paradigm enabled accurate and robust control of prosthesis WFE and WPS across a large repertoire of tasks performed at different arm configurations (Figs 3-7, Movie 1). Moreover, results showed the ability of natural control of WPS and HOC during functionally relevant clothespin tests (Figs 8, Movies 2-3) and object manipulation tests (Movies 4-7). These tests underwent

1
2 434 dynamic stump-prosthesis movements, enabling testing robustness to EMG non-stationarities (due relative
3
4 435 movement between muscle fiber and electrodes) and control precision in the force domain. For all subjects,
5
6 436 model calibration (Fig. 2) was always performed a number of days prior to real-time prosthesis control
7
8 437 experiments. This provided evidence of the framework ability of retaining subject-specific parameter
9
10 438 consistency across time scales, i.e. the model needed to be established once for all per subject. Subjects
11
12 439 controlled the prosthesis throughout three series of tasks including: virtual target reaching, clothespin, and
13
14 440 functional tasks. This Section presents quantitative results as well as the framework computational times
15
16 441 across all series of tasks. In the remainder of this section the three intact-limbed individuals will be referred to
17
18 442 as IL1, IL2, and IL3 respectively. The transradial amputee will be referred to as TR1 as indicated in Table II.
19
20
21 443
22

23 444 **Virtual Target Reaching Tasks**

24
25 445 The virtual target reaching tasks tested whether the proposed framework enabled subjects to control
26
27 446 prosthesis WFE and WPS individually, sequentially, as well as simultaneously. Subjects sat in front of a
28
29 447 monitor and were instructed to move a virtual ball-shaped cursor to reach a square-shaped target and keep
30
31 448 the cursor within the target for ~1 second. Cursor movements were accomplished by actuating prosthesis
32
33 449 WFE and WPS DOFs via forearm muscle contractions. Since it is known that arm posture greatly affects the
34
35 450 performance of state of the art decoders [2], we quantified our system robustness to arm configuration, i.e.
36
37 451 each test was repeated with the right arm in three postures: (a) fully extended elbow, (b) 90-degree flexed
38
39 452 elbow, and (c) 90-degree flexed elbow and 90-degree abducted shoulder.
40
41

42 453 During the virtual target reaching tasks subjects reached a total of 672 targets, i.e. 168 targets per subjects
43
44 454 on average. The first three series of tests verified the precision in controlling WFE and WPS individually
45
46 455 (i.e. first and second series, see Methods Section) as well as sequentially (i.e. third series, see Methods
47
48 456 Section) in order to reach vertically and/or horizontally displayed targets. Importantly, in all three series, the
49
50 457 system always allowed simultaneous DOF control, but subjects were instructed to activate the DOFs
51
52 458 individually, testing thereby the ability for selective control. Fig. 3 depicts vertical and horizontal reaching
53
54 459 trajectories (i.e. individual DOF control) reported for TR1 along with recorded EMGs and estimated WFE
55
56 460 and WPS moments driving the prosthesis movement. Subjects always reached targets using linear
57
58 461 trajectories thereby successfully actuating a single DOF at a time with high precision. Path similarity was
59
60 462 always accomplished with $R^2 > 0.98$ across all targets and subjects. Intact-limbed individuals and transradial

1
2 463 amputee reached all targets with comparable times (median\interquartile range) during the individual and
3
4 464 sequential DOF (two DOFs controlled in sequence) control tasks: 2.2\1.6s (individual) and 4.6\3.1s
5
6 465 (sequential) across IL1-3 whereas 2.3\1.6s (individual) and 7.1\5.1s (sequential) for TR1.

8 466 The fourth series of tests verified the system ability to enable controlling WFE and WPS simultaneously.
9
10 467 Movie 1 shows the proposed model-based framework operated in real-time for the control of the prosthesis
11
12 468 by IL1, displaying both musculoskeletal model, recorded EMGs and estimated wrist moments. The movie
13
14 469 also shows the concurrent control of the ball-shaped cursor for reaching a variety of diagonal targets (see
15
16 470 user interface on external screen). Note that the cursor diagonal trajectories directly correspond to the
17
18 471 prosthesis simultaneous actuation of WPS and WFE. Fig. 4 further depicts diagonal reaching trajectories
19
20
21 472 reported for TR1 along with recorded EMGs and estimated WFE and WPS moments driving the prosthesis
22
23 473 movement. Fig. 4 shows highly coupled production of WFE and WPS moments underlying simultaneous
24
25 474 control of prosthesis DOFs. Moment generating patterns were substantially different during the sequential
26
27 475 DOF tasks (Fig. 3), i.e. reduced degree of WFE and WPS moment coupling. Fig. 5 depicts representative
28
29 476 diagonal reaching trajectories for all intact-limbed individuals. Figs 4 and 5 also show that all subjects were
30
31 477 able to produce diagonal trajectories. Moreover, each individual displayed ability of generating optimal
32
33 478 diagonal trajectories in specific quadrants. TR1 was particularly capable of generating diagonal trajectories
34
35 479 in quadrants 1, 3 and 4. IL1 and IL3 were capable of generating diagonal trajectories across all quadrants
36
37 480 whereas IL2 in quadrants 2 and 4.

38
39
40 481 Intact-limbed individuals and transradial amputee reached all targets with comparable times
41
42 482 (median\interquartile range), i.e. 3.8\2.8s across IL1-3 and 5.3\4.7s for TR1. Each individual reached targets
43
44 483 with substantially less time using our proposed model-based framework (model-based) than when using the
45
46 484 classic commercially available two-channel sequential control scheme based on co-contraction (classic). Figs
47
48 485 6A and 6B respectively reports the distribution and median\interquartile range of reaching times across all
49
50 486 targets on a subject-specific basis. Across all subjects, quadrant 1 targets were reached (median\interquartile
51
52 487 range) in 3.4\2.9s (model-based) and 6.2\3.4s (classic). Quadrant 2 targets were reached in 4.1\3.4s (model-
53
54 488 based) and 5.9\2.6s (classic). Quadrant 3 targets were reached in 3.4\2.2s (model-based) and 7.4\3.7s
55
56 489 (classic). Quadrant 4 targets were reached in 4.2\3.9s (model-based) and 5.8\2.4s (classic).

57
58
59 490 Importantly, the performance of the proposed model-based approach was preserved across all arm
60
61 491 postures. Fig. 7 reports reaching times across arm postures and specifically for each subject. This shows our

proposed model-based approach has no performance decay across arm configuration and consistently outperforms the robust classic control scheme. In this, reaching times were always smaller using the model-based approach than when using the classic control scheme. Across all subjects, reaching times during extended elbow posture were (median\interquartile range) 3.1\2.2s (model-based) and 7.1\3.8s (classic). During elbow flexed arm posture they were 3.4\3s (model-based) and 6.2\4.9s (classic). Finally, during elbow flexed and shoulder abducted arm posture they were 3.3\2s (model-based) and 5.9\3.7s (classic).

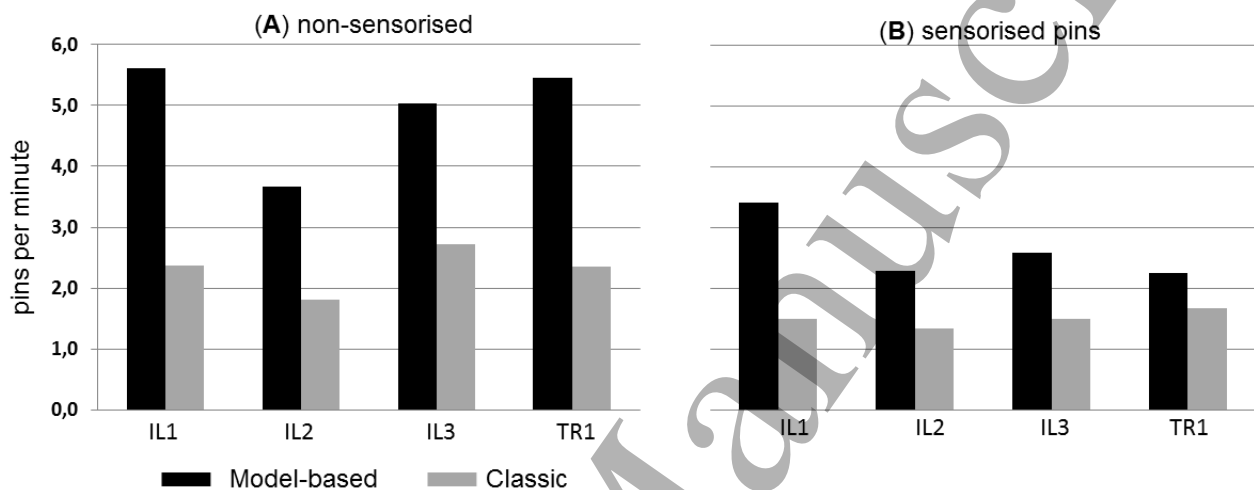


Figure 8. Speed performance during clothespin test. Performance is evaluated in terms of number of clothespins correctly picked and placed per minute (ppm) both using our proposed system (model-based) and the commercially available system (classic). Results are reported for three intact-limbed individuals (IL1-3) and one transradial amputee (TR1). Also refer to Table II. (A) Results are reported for the non-sensorised pin test. (B) Performance is evaluated in terms of number of sensorised clothespins correctly picked without triggering light sensor.

Clothespin Task

The clothespin task verified the ability to accurately control WPS and HOC simultaneously and proportionally across functionally relevant tasks. Subjects performed two series of tests with different pin types. Subjects picked a total of 48 non-sensorised pins (i.e. 12 pins per subject) and a total of 20 sensorized pins (i.e. 5 pins per subject).

The first series of tests (Movie 2, Fig. 8A) involved picking and placing non-sensorised pins (see Methods Section). Pins were arranged in four triplets of different stiffness as previously reported [44].

1
2 514 Results showed that both intact-limbed and amputee individuals could control prosthesis WPS and HOC
3
4 515 simultaneously while generating natural motions. This enabled individuals to complete the test with an
5
6 516 average speed of 5.24 ± 0.9 pins per minute (ppm) using the proposed model-based framework. In this, the
7
8 517 amputee's speed performance (5.5 ± 0.4 ppm) was comparable to that of subject IL1 (5.6 ± 0.7 ppm) and higher
9
10 518 than that of subjects IL2 (3.67 ± 0.5 ppm) and IL3 (5.03 ± 0.6 ppm). Each individual completed the test with
11
12 519 substantially better performance than when they used the commercially available sequential control scheme
13
14 520 based on co-contraction (Fig. 8A) [9]. For the classic-control scheme, average speed performance was
15
16 521 2.3 ± 0.4 ppm and ranged between 1.8 ± 0.1 ppm (subject IL2) and 2.7 ± 0.2 ppm (subject IL3).
17
18

19 522 The second series (Movie 3, Fig. 8B) involved picking and placing sensorised pins equipped with
20
21 523 custom-made contact sensors. The sensor registered when the pin was grasped with force levels beyond
22
23 524 predefined thresholds. This was indicated by activating a LED signaling that the subject would have
24
25 525 "broken" the grasped object in the real world. Similarly to the first series, test underlay five pins of different
26
27 526 stiffness as previously reported (see Material and Methods Section) [44]. The aim was to pick each pin while
28
29 527 accurately controlling grasping force in order to open the pin enough to remove it from the bar but without
30
31 528 using excessive forces, which would trigger the light sensor. The target force windows to successfully
32
33 529 relocate each pin were 7-15% (yellow pins in Movies 2-3), 13-23% (red pins in Movies 2-3), 23-32% (green
34
35 530 pins in Movies 2-3), and 35-43% (black pins in Movies 2-3) of the prosthesis maximum force. Results
36
37 531 revealed each individual's ability of fine controlling the prosthesis grip force while simultaneously
38
39 532 controlling hand rotation. Movie 3 shows the amputee's ability of grasping sensorized pins with the
40
41 533 appropriate force level while preserving the required force level accurately during prosthesis wrist pronation-
42
43 534 supination, hence with no unwanted activations, i.e. no cross talk across DOFs. Individuals completed the
44
45 535 sensorized clothespin test with an average speed of 2.7 ± 0.4 pins per minute (ppm) using the proposed model-
46
47 536 based framework (Fig. 9). In this, the amputee's speed performance (2.25 ± 0.1 ppm) was comparable to that
48
49 537 of intact-limbed subject IL2 (2.28 ± 0.2 ppm) IL3 (2.58 ± 0.2 ppm) while IL1 (3.4 ± 0.2 ppm) displayed the best
50
51 538 performance. Similarly to the first test, each individual completed the test with better performance than when
52
53 539 they used the commercially available sequential control scheme based on co-contraction (Fig. 9) [9]. For the
54
55 540 classic-control scheme, average speed performance was 1.5 ± 0.13 ppm and ranged between 1.3 ppm (subject
56
57 541 IL2) and 1.6 ppm (subject TR1).
58
59
60

542

543 **Functional Tasks**

544 The functional tasks verified the system ability of performing real-world functions robustly and intuitively
545 and were performed only with the proposed model-based control scheme. Results are reported in the form of
546 a large repertoire of videos. In this, the transradial amputee could successfully perform tasks involving fine
547 control actions (Movies 4-5) as well as manipulation of different objects (Movies 6-7). Fine control actions
548 are displayed in Movie 4, showing TR1 executing a block-turn task involving fine control of HOC and WPS
549 DOFs in the precise positioning of a narrow wooden block in equilibrium on a wooden shelf. Movie 5 shows
550 TR1 precisely controlling HOC DOF force for grasping an egg. The movie shows TR1 ability of grasping
551 force fine control while rotating the prosthetic wrist without breaking the egg. It is worth stressing that this
552 task was performed with no force feedback provided to the amputee. Movie 7 shows how our proposed
553 system was transparent to mechanically induced EMG movement artefacts, preventing inadvertently
554 activating the prosthesis DOFs, i.e. by the resulting noise. Remarkably, the proposed system always enabled
555 amputee's voluntary prosthesis control under high movement-artefact contaminated condition. Finally, the
556 system proved to be robust to highly dynamic movements including grasping and manipulating heavy
557 objects (i.e. a 1.5L water bottle, Movie 7), a tasks that would be challenging for state of the art non-invasive
558 myoelectric systems due to underlying alterations in EMG patterns in response to object weight [2,9,11].

560 **Computational Time**

561 Across all subjects and tests the proposed framework generated prosthesis control commands with average
562 speeds 35 ± 11 ms. This includes the total net delay from the EMG recording to final prosthesis actuation. In
563 this, 90% of control commands produced in one single time frame were generated within 55ms. This is well
564 within the human perceivable delay in motor execution [45,46].

566 **DISCUSSION**

567 We presented a paradigm of man-machine interfacing where the complete information extracted from an
568 individual's composite neuromusculoskeletal system (i.e. from neuromuscular activation to skeletal joint
569 mechanics) is used to control a robotic multi-functional prosthetic limb. We tested this paradigm on three
570 intact-limbed individuals and on one transradial amputee during a range of tasks involving real-time control

1
2 571 of a physical prosthesis. The results showed performance and control capabilities superior than state of the
3
4 572 art non-invasive myocontrol approaches.
5

6 573 Our proposed neuro-mechanical interface addressed a major limit in current state of the art decoders, i.e.
7
8 574 the inability of synthesizing the mechanisms that the neuro-musculo-skeletal system uses to control
9
10 575 biological joints. State of the art consolidated approaches to the control of artificial limbs are based on
11
12 576 machine learning for establishing a single mapping function between EMG and joint kinematics. In this
13
14 577 context, there currently exist commercial systems based on pattern recognition (e.g. Coapt LLC) that showed
15
16 578 important clinical use [47,48]. Moreover, recent regression based methods have shown levels of robustness
17
18 579 to noise [49]. However, current machine learning approaches still display sensitivity to electrode
19
20 580 replacement as well as lack of robustness to arm postures, thus providing control paradigms that are sensitive
21
22 581 to external conditions.
23
24

25 582 We propose an alternative idea based on a biomimetic model-based decoder, i.e. a computational model
26
27 583 that explicitly synthesizes the dynamics of the musculo-skeletal system as controlled by neural surrogates,
28
29 584 i.e. EMG-derived muscle activation signals (Fig. 1). Although online modelling was previously employed in
30
31 585 lower limb prostheses [50] and robotic exoskeleton [51,52] scenarios, our study proposes a paradigm never
32
33 586 presented for online myoelectric prosthesis control in transradial amputees. Forearm EMG recordings are
34
35 587 used to drive forward physiologically correct models of the human musculoskeletal system in real-time,
36
37 588 rather than regressing “all the way to” joint angles. This provides a completely new approach to decode
38
39 589 amputees’ phantom limb function and concurrently control upper limb prostheses. This model-based
40
41 590 biomimetic approach enabled for the first time decoding a transradial amputee’s phantom limb mechanical
42
43 591 moments (Figs 3-4) and concurrently mimicking biological wrist function in artificial limbs in real-time
44
45 592 (Movies 1-7). Whether joint moments could be reliably decoded from an amputee’s residual muscles EMG
46
47 593 to robustly control a prosthetic wrist-hand represented an unanswered scientific question that this work
48
49 594 directly addressed. In our paradigm, the prosthesis is the physical device that converted EMG-predicted joint
50
51 595 moments into joint angles, thus eliminating the need for numerically integrating dynamic equations of
52
53 596 motions. This is different from current solutions operating at the kinematic-level, including (1) model-free
54
55 597 decoders, sensitive to unseen motor tasks and time scales [5] and model-based methods [21] that integrate
56
57 598 forward dynamic equations of motion, which is a computationally expansive and numerically unstable step
58
59 599 [23].
60

1
2 600 Removing the need for integrating the equation of motion is central for simulating large-scale models, an
3
4 601 important element especially relevant for individuals who underwent targeted muscle reinnervation surgical
5
6 602 procedures, who require regaining control of large sets of skeletal DOFs. Our proposed biomimetic model-
7
8 603 based approach enables control intuitiveness. In this, subjects do not have to learn to produce a specific
9
10 604 EMG pattern for prosthesis control. They only need to move their own biological or phantom limb, whose
11
12 605 mechanical function is directly captured by the neuro-mechanical interface and concurrently rendered in the
13
14 606 real-world by the controlled prosthetic limb.

16
17 607 Results have demonstrated that our method provided an advanced and reliable prosthesis control across
18
19 608 tests involving reaching ~600 virtual targets from three arm postures, manipulation of 48 non-sensorised
20
21 609 clothespins, 20 sensorised clothespins as well as manipulation of real-world objects during tasks mimicking
22
23 610 daily living scenarios. The subjects could successfully activate prosthesis DOFs simultaneously (WFS and
24
25 611 WPS, WPS and HOC) across a large range of tasks, and they could proportionally modulate the ratio of the
26
27 612 DOF activations, as demonstrated by the diagonal trajectories with different slopes in Figs 4-5. Furthermore,
28
29 613 subjects successfully activated single DOFs and transitioned between DOFs sequentially, with minimal cross
30
31 614 talk between DOF-specific command signals, which has shown to be a challenge for regression-based
32
33 615 methods [53]. Our method consistently and significantly outperformed commercially available benchmark
34
35 616 systems (i.e. robust two channel command interface, commercial benchmark) during multi-DOF tasks but
36
37 617 also during single-DOF tasks where commercial benchmarks would be expected to best perform. This was
38
39 618 evident in the case of the amputee subject, an especially encouraging result.

41
42 619 Fig. 3 shows that in some cases, subjects did not reach a given target via a single muscle contraction but
43
44 620 rather via a sequence of brief contractions. This resulted in a number of trajectories underling a sequence
45
46 621 torque pulses, dictating virtual cursor movement along a straight path with a variable velocity. Future work
47
48 622 will assess whether practice will enable subjects to minimize the number of contractions needed to reach a
49
50 623 give target. Fig. 4, shows that certain DOF combinations were achieved via minimally overlapped moment
51
52 624 curves. While this is in line with literature studies on natural wrist rotations [54–58], it may also be a
53
54 625 consequence of the fact that certain DOF-combinations are more intuitive than others. This may be
55
56 626 especially relevant for the amputee subject who performed the tasks with no visual feedback on the
57
58 627 prosthesis (please see Movie 1). Future work will also assess to what extent the lack of intrinsic muscle
59
60 628 EMGs may contribute to decoded joint moments across coordinated wrist-hand tasks.

1
2 629 Our proposed approach demonstrated decoding robustness across a large variety of wrist-hand tasks
3
4 630 (Movie 1) performed across different arm configurations (Figs. 6-7), and during dynamic tasks (i.e. Movies
5
6 631 4-7). Movie 6 demonstrated our system ability to generate no unwanted prosthesis movement when EMG
7
8 632 electrode cables underwent mechanically induced movement artefacts. Although this is not representative of
9
10 633 commercially available systems schemes (i.e. involving no external cables that could be perturbed), these
11
12 634 results show the potential robustness of our system to external movement artefact that may nevertheless
13
14 635 come from interaction with the environment. Moreover, it enabled performing highly dynamic motor tasks
15
16 636 including manipulating heavy objects (Movie 7).

17
18
19 637 Our system robustness (which was comparable to the most robust benchmark system in the market)
20
21 638 derived from the fact that any joint moment estimate must always exist within the musculoskeletal model
22
23 639 operational space and be therefore physiologically plausible. This cannot be achieved with current machine
24
25 640 learning decoders that, when trained in one condition, would produce unrealistic estimates (i.e. outside the
26
27 641 physiological space) in novel conditions. Machine learning decoding solutions are not constrained by any
28
29 642 physiologically plausible structure. Our proposed approach establishes a subject-specific model of an
30
31 643 individual's musculoskeletal system. In this, the musculoskeletal model linear scaling and parameter non-
32
33 644 linear calibration (i.e. see Methods Section, Fig. 2) directly determine how EMG signals are processed by the
34
35 645 subject's musculoskeletal system, i.e. how they are converted into muscle force and further projected onto
36
37 skeletal DOFs. This effectively reduces the space of potential solutions as EMGs can be mapped only onto
38 646 mechanical forces that are contained within the musculoskeletal model operational space. Current methods
39
40 647 map EMG signals into control commands with no physiological constraints, thus dealing with large solution
41
42 648 spaces that contain large portions of non-physiologically plausible solutions.

43
44 649
45
46 650 Results were obtained on a small number of subjects. Future work will be directed in testing the
47
48 651 generalization of the results to a greater population encompassing subjects with different levels of
49
50 652 amputations as well as comparison of our methodology with respect to state-of-the-art pattern recognition
51
52 653 techniques. Our proposed method demonstrated applicability in amputees who underwent traumatic injuries.
53
54 654 Future work will assess whether this method can be translated to individuals affected by congenital limb
55
56 655 absence. This will require a systematic research to investigate whether motor task learning can be induced in
57
58 656 such individuals undergoing physiotherapy training coupled with the proposed real-time system. Further
59
60 657 research is also needed to investigate to what extent Hill-type muscle models may contribute to reduce EMG

1
2 658 noise artefacts in online myocontrol scenarios. In this context, computational muscle models may enable
3
4 659 simulating musculotendon viscoelasticity, which may act as a dynamic filter for reducing the impact of noise
5
6 660 remaining in the EMG after linear envelope computation. Although our results provided evidence of
7
8 661 robustness to arm configurations further work is necessary to assess robustness to other sources of noise.
9
10 662 Future work will also perform systematic analyses to quantify to what extent the model scaling and
11
12 663 calibration procedures (see Methods Section) can be retained for a subject across time scales, i.e. involving
13
14 664 longitudinal testing over a number of consecutive weeks.
15
16
17 665

18 666 **CONCLUSION**

20
21 667 This study showed the potential of the proposed control method to enable the first real-time multi-DOF
22
23 668 myoelectric technology that decodes an amputee's phantom limb musculoskeletal mechanics and could be
24
25 669 employed in real-world scenarios to control a total of three DOFs including forearm pronation-supination,
26
27 670 wrist flexion-extension and hand opening-closing. Future work will couple our proposed model-based
28
29 671 approach with deconvolution-based decoding of motor neuron discharges from high-density
30
31 672 electromyograms and enable bionic limb control in higher-dimensional DOF spaces [1,30]. Integrating
32
33 673 model-based paradigms as a mechanism to constrain and control prosthetic wrist-hand rotation within
34
35 674 physiologically plausible operational spaces has the potential to bring prosthetic technology closer to match
36
37 675 biological joint function with implications for both upper and lower limb rehabilitation technologies. It will
38
39 676 enable individuals to control artificial limbs by estimating physiological activations in their residual muscles,
40
41 677 hence control intuitiveness. It will enable decoding "any" movement (i.e. not only those learned in a specific
42
43 678 regime) because it synthesizes the underlying neuromuscular processes, hence control robustness and
44
45 679 extrapolation to unseen conditions. It will enable predicting internal somatosensory variables (i.e.
46
47 680 muscle/tendon length, tension), which will help restore amputees' somatosensory processes in advanced
48
49 681 closed-loop neuro-prostheses.
50
51
52 682

53 683 **REFERENCES**

- 54
55 684 [1] Farina D, Vujaklija I, Sartori M, Kapelner T, Negro F, Jiang N, Bergmeister K, Andalib A, Principe
56
57 685 J and Aszmann O C 2017 Man/machine interface based on the discharge timings of spinal motor
58
59 686 neurons after targeted muscle reinnervation *Nat. Biomed. Eng.* **1** 0025

- 1
2 687 [2] Farina D and Aszmann O 2014 Bionic Limbs: Clinical Reality and Academic Promises. *Sci. Transl.*
3
4 688 *Med.* **6** 257ps12
- 5
6 689 [3] Micera S, Rossini P M, Rigosa J, Citi L, Carpaneto J, Raspopovic S, Tombini M, Cipriani C,
7
8 690 Assenza G, Carrozza M C, Hoffmann K-P, Yoshida K, Navarro X and Dario P 2011 Decoding of
9
10 691 grasping information from neural signals recorded using peripheral intrafascicular interfaces. *J.*
11
12 692 *Neuroeng. Rehabil.* **8** 53
- 13
14
15 693 [4] Kuiken T A, Miller L A, Lipschutz R D, Lock B A, Stubblefi K, Marasco P D, Zhou P, Dumanian G
16
17 694 A, Stubblefield K, Marasco P D, Zhou P and Dumanian G A 2007 Targeted reinnervation for
18
19 695 enhanced prosthetic arm function in a woman with a proximal amputation: a case study. *Lancet* **369**
20
21 696 371–80
- 22
23 697 [5] Jiang N, Dosen S, Muller K R and Farina D 2012 Myoelectric Control of Artificial Limbs: Is There a
24
25 698 Need to Change Focus? [In the Spotlight] *IEEE Signal Process. Mag.* **29** 150–2
- 26
27 699 [6] Hahne J M, Bießmann F, Jiang N, Rehbaum H, Member S, Farina D, Member S, Meinecke F C,
28
29 700 Müller K and Parra L C 2014 Linear and Nonlinear Regression Techniques for Simultaneous and
30
31 701 Proportional Myoelectric Control **22** 269–79
- 32
33 702 [7] Farina D, Jiang N, Rehbaum H, Holobar A, Graimann B, Dietl H and Aszmann O C 2014 The
34
35 703 extraction of neural information from the surface EMG for the control of upper-limb prostheses:
36
37 704 Emerging avenues and challenges *IEEE Trans. Neural Syst. Rehabil. Eng.* **22** 797–809
- 38
39
40 705 [8] Enoka R M 2008 *Neuromechanics of Human Movement* (Human Kinetics Publishers, Inc.)
- 41
42 706 [9] Jiang N, Dosen S, Muller K R and Farina D 2012 Myoelectric Control of Artificial Limbs: Is There a
43
44 707 Need to Change Focus? [In the Spotlight] *IEEE Signal Process. Mag.* **29** 150–2
- 45
46 708 [10] Ifft P J, Shokur S, Li Z, Lebedev M a and Nicolelis M a L 2013 A brain-machine interface enables
47
48 709 bimanual arm movements in monkeys. *Sci. Transl. Med.* **5** 210ra154
- 49
50 710 [11] Sartori M, Llyod D G and Farina D 2016 Neural Data-driven Musculoskeletal Modeling for
51
52 711 Personalized Neurorehabilitation Technologies *IEEE Trans. Biomed. Eng.* **63** 879–93
- 53
54 712 [12] Lloyd D G and Besier T F 2003 An EMG-driven musculoskeletal model to estimate muscle forces
55
56 713 and knee joint moments in vivo *J. Biomech.* **36** 765–76
- 57
58
59 714 [13] Sartori M, Reggiani M, Farina D and Lloyd D G 2012 EMG-driven forward-dynamic estimation of
60
715 muscle force and joint moment about multiple degrees of freedom in the human lower extremity

1
2 716 *PLoS One* **7** 1–11

- 3
4 717 [14] Sartori M, Farina D and Lloyd D G 2014 Hybrid neuromusculoskeletal modeling to best track joint
5
6 718 moments using a balance between muscle excitations derived from electromyograms and
7
8 719 optimization *J. Biomech.* **47** 3613–21
- 9
10 720 [15] Durandau G, Farina D and Sartori M 2018 Robust Real-Time Musculoskeletal Modeling driven by
11
12 721 Electromyograms *IEEE Trans. Biomed. Eng.* **65** 556–64
- 13
14 722 [16] Manal K, Gravare-Silbernagel K and Buchanan T S 2011 A real-time EMG-driven musculoskeletal
15
16 723 model of the ankle *Multibody Syst. Dyn.* **28** 169–80
- 17
18 724 [17] Pizzolato C, Reggiani M, Saxby D J, Ceseracciu E, Modenese L and Lloyd D G 2017 Biofeedback
19
20 725 for Gait Retraining Based on Real-Time Estimation of Tibiofemoral Joint Contact Forces *IEEE*
21
22 726 *Trans. Neural Syst. Rehabil. Eng.* **25** 1612–21
- 23
24 727 [18] Manal K, Gonzalez R V, Lloyd D G and Buchanan T S 2002 A real-time EMG-driven virtual arm.
25
26 728 *Comput. Biol. Med.* **32** 25–36
- 27
28 729 [19] Chadwick E K, Blana D, van den Bogert A J T and Kirsch R F 2009 A real-time, 3-D
29
30 730 musculoskeletal model for dynamic simulation of arm movements. *IEEE Trans. Biomed. Eng.* **56**
31
32 731 941–8
- 33
34 732 [20] Crouch D L and He H 2016 Lumped-parameter electromyogram-driven musculoskeletal hand
35
36 733 model: A potential platform for real-time prosthesis control *J. Biomech.* **49** 3901–7
- 37
38 734 [21] Crouch D L and Huang H (Helen) 2017 Musculoskeletal model-based control interface mimics
39
40 735 physiologic hand dynamics during path tracing task *J. Neural Eng.* **14** 036008
- 41
42 736 [22] Pan L, Crouch D L and Huang H 2018 Myoelectric Control Based on a Generic Musculoskeletal
43
44 737 Model: Toward a Multi-User Neural-Machine Interface *IEEE Trans. Neural Syst. Rehabil. Eng.* **26**
45
46 738 1435–42
- 47
48 739 [23] Blana D, Chadwick E K, van den Bogert A J and Murray W M 2017 Real-time simulation of hand
49
50 740 motion for prosthesis control *Comput. Methods Biomech. Biomed. Engin.* **20** 540–9
- 51
52 741 [24] Durandau G, Farina D and Sartori M Real-time musculoskeletal modeling driven by
53
54 742 electromyograms *IEEE Trans. Biomed. Eng.*
- 55
56 743 [25] Schaffelhofer S, Sartori M, Scherberger H and Farina D 2015 Musculoskeletal Representation of a
57
58 744 Large Repertoire of Hand Grasping Actions in Primates *IEEE Trans. Neural Syst. Rehabil. Eng.* **23**

- 1
2 745 210–20
3
- 4 746 [26] Sartori M, Reggiani M, Pagello E and Lloyd D G 2012 Modeling the human knee for assistive
5
6 747 technologies. *IEEE Trans. Biomed. Eng.* **59** 2642–9
7
- 8 748 [27] Sartori M, Reggiani M, van den Bogert A J and Lloyd D G 2012 Estimation of musculotendon
9
10 749 kinematics in large musculoskeletal models using multidimensional B-splines *J. Biomech.* **45** 595–
11
12 750 601
13
- 14 751 [28] Sartori M, Maculan M, Pizzolato C, Reggiani M and Farina D 2015 Modeling and Simulating the
15
16 752 Neuromuscular Mechanisms regulating Ankle and Knee Joint Stiffness during Human Locomotion *J.*
17
18 753 *Neurophysiol.* **114** 2509–27
20
- 21 754 [29] Sartori M, Llyod D G and Farina D 2016 Neural data-driven musculoskeletal modeling for
22
23 755 personalized neurorehabilitation technologies *IEEE Trans. Biomed. Eng.* **63** 879–93
24
- 25 756 [30] Sartori M, Yavuz U S and Farina D 2017 In Vivo Neuromechanics: Decoding Causal Motor Neuron
26
27 757 Behavior with Resulting Musculoskeletal Function *Sci. Rep.* **7** 13465
28
- 29 758 [31] Besier T F, Lloyd D G and Ackland T R 2003 Muscle activation strategies at the knee during
30
31 759 running and cutting maneuvers. *Med. Sci. Sports Exerc.* **35** 119–27
32
- 33 760 [32] Manal K and Buchanan T S 2003 A one-parameter neural activation to muscle activation model:
34
35 761 estimating isometric joint moments from electromyograms. *J. Biomech.* **36** 1197–202
37
- 38 762 [33] Shao Q, Bassett D N, Manal K and Buchanan T S 2009 An EMG-driven Model to Estimate Muscle
39
40 763 Forces and Joint Moments in Stroke Patients *Comput. Biol. Med.* **39** 1083–8
41
- 42 764 [34] Higginson J S, Ramsay J W and Buchanan T S 2012 Hybrid models of the neuromusculoskeletal
43
44 765 system improve subject-specificity *Proc. Inst. Mech. Eng. Part H J. Eng. Med.* **226** 113–9
45
- 46 766 [35] Manal K and Buchanan T S 2005 Use of an EMG-driven biomechanical model to study virtual
47
48 767 injuries. *Med. Sci. Sports Exerc.* **37** 1917–23
49
- 50 768 [36] Barrett R, Besier T and Lloyd D 2007 Individual muscle contributions to the swing phase of gait: An
51
52 769 EMG-based forward dynamics modelling approach *Simul. Model. Pract. Theory* **15** 1146–55
53
- 54 770 [37] Hayashibe M and Guiraud D 2013 Voluntary EMG-to-force estimation with a multi-scale
55
56 771 physiological muscle model. *Biomed. Eng. Online* **12** 86
58
- 59 772 [38] Delp S L, Anderson F C, Arnold A S, Loan P, Habib A, John C T, Guendelman E and Thelen D G
60
773 2007 OpenSim: open-source software to create and analyze dynamic simulations of movement. *IEEE*

- 1
2 774 *Trans. Biomed. Eng.* **54** 1940–50
3
- 4 775 [39] Saul K R, Hu X, Goehler C M, Vidt M E, Daly M, Velisar A and Murray W M 2014 Benchmarking
5
6 776 of dynamic simulation predictions in two software platforms using an upper limb musculoskeletal
7
8 777 model. *Comput. Methods Biomech. Biomed. Engin.* 1–14
9
- 10 778 [40] H.J. Hermens and B Freriks 2017 SENIAM Project *SENIAM Proj.* 1
11
- 12 779 [41] Sartori M, Gizzi L, Lloyd D G D G and Farina D 2013 A musculoskeletal model of human
13
14 780 locomotion driven by a low dimensional set of impulsive excitation primitives *Front. Comput.*
15
16 781 *Neurosci.* **7** 79
17
- 18 782 [42] Sartori M, Maculan M, Pizzolato C, Reggiani M and Farina D 2015 A Theoretical and
19
20 783 Computational Framework for Modeling and Simulating Musculoskeletal Stiffness during
21
22 784 Locomotion *The 25th Congress of the International Society of Biomechanics* (Glasgow) pp 1–2
23
24 785 [43] Amsuess S, Vujaklija I, Gobel P, Roche A, Graimann B, Aszmann O and Farina D 2015 Context-
25
26 786 Dependent Upper Limb Prosthesis Control for Natural and Robust Use *IEEE Trans. Neural Syst.*
27
28 787 *Rehabil. Eng.* **4320** 1–1
29
30 788 [44] De Nunzio A M, Dosen S, Lemling S, Markovic M, Schweisfurth M A, Ge N, Graimann B, Falla D
31
32 789 and Farina D 2017 Tactile feedback is an effective instrument for the training of grasping with a
33
34 790 prosthesis at low- and medium-force levels *Exp. Brain Res.* **235** 2547–59
35
36 791 [45] Farina D and Sartori M 2016 Surface Electromyography for Man-Machine Interfacing in
37
38 792 Rehabilitation Technologies *Surface Electromyography: Physiology, Engineering and Applications*
39
40 793 ed D Farina and R Merletti (IEEE/Wiley) pp 540–60
41
42 794 [46] Parker P, Englehart K and Hudgins B 2006 Myoelectric signal processing for control of powered
43
44 795 limb prostheses *J. Electromyogr. Kinesiol.* **16** 541–8
45
46 796 [47] Kuiken T, Turner K, Soltys N and Dumanian G 2015 First clinical fitting of an individual after
47
48 797 bilateral TMR with pattern recognition control *Prosthet. Orthot. Int.* **39** 133
49
50 798 [48] Hargrove L J, Miller L A, Turner K and Kuiken T A 2017 Myoelectric Pattern Recognition
51
52 799 Outperforms Direct Control for Transhumeral Amputees with Targeted Muscle Reinnervation: A
53
54 800 Randomized Clinical Trial *Sci. Rep.* **7**
55
56 801 [49] Hahne J M, Markovic M and Farina D 2017 User adaptation in Myoelectric Man-Machine Interfaces
57
58 802 *Sci. Rep.* **7**

- 1
2 803 [50] Eilenberg M F, Geyer H and Herr H 2010 Control of a powered ankle-foot prosthesis based on a
3
4 804 neuromuscular model. *IEEE Trans. Neural Syst. Rehabil. Eng.* **18** 164–73
5
6 805 [51] Fleischer C and Hommel G 2008 A Human – Exoskeleton Interface Utilizing Electromyography
7
8 806 *IEEE Trans. Robot.* **24** 872–82
9
10 807 [52] Cavallaro E E, Rosen J, Perry J C and Burns S 2006 Real-Time Myoprocessors for a Neural
11
12 808 Controlled Powered Exoskeleton Arm *IEEE Trans. Biomed. Eng.* **53** 2387–96
13
14 809 [53] Farina D, Vujaklija I, Sartori M, Kapelner T, Negro F, Jiang N, Bergmeister K, Andalib A, Principe
15
16 810 J and Aszmann O 2016 Man-Machine Interfacing With Discharge Timings of Spinal Motor Neurons
17
18 811 After Targeted Muscle Reinnervation *Nat. Biomed. Eng.*
19
20
21 812 [54] Formica D, Charles S K, Zollo L, Guglielmelli E, Hogan N and Krebs H I 2012 The passive stiffness
22
23 813 of the wrist and forearm *J. Neurophysiol.* **108** 1158–66
24
25 814 [55] Charles S K and Hogan N 2011 Dynamics of wrist rotations *J. Biomech.* **44** 614–21
26
27 815 [56] Rankin J W and Neptune R R 2012 Musculotendon lengths and moment arms for a three-
28
29 816 dimensional upper-extremity model. *J. Biomech.* **45** 1739–44
30
31 817 [57] Holzbaur K R S, Murray W M and Delp S L 2005 A Model of the Upper Extremity for Simulating
32
33 818 Musculoskeletal Surgery and Analyzing Neuromuscular Control *Ann. Biomed. Eng.* **33** 829–40
34
35 819 [58] Peadar A W and Charles S K 2014 Dynamics of wrist and forearm rotations *J Biomech* **47** 2779–85
36
37
38 820
39

40 821 **COMPETING INTERESTS**

41
42 822 The authors declare no financial competing interests.
43
44 823
45

46 824 **PARTICIPANT CONSENT**

47
48 825 The authors have confirmed that any identifiable participants in this study have given their consent for
49
50 826 publication.
51
52 827
53

54 828 **DATA AND MATERIALS AVAILABILITY**

55
56 829 Data and code are available upon request.
57
58
59 830
60

831 **MOVIES**

1
2 832 **Movie 1. Graphical user interface during wrist control tasks.** The proposed model-based framework
3
4 833 operated in real-time for the simultaneous control of the prosthesis wrist flexion-extension (WFE) and
5
6 834 pronation-supination (WPS) by IL1 (Table II). The movie displays the musculoskeletal model, recorded
7
8 835 EMGs and estimated joint moments (see laptop) and the concurrent control of the ball-shaped cursor for
9
10 836 reaching a variety of diagonal targets (see user interface on external screen). Note that the cursor diagonal
11
12 837 trajectories directly correspond to the prosthesis simultaneous actuation of WPS and WFE. After every target
13
14 838 is successfully reached, the prosthesis automatically resets to its neutral position.

15
16
17 839
18
19 840 **Movie 2. Non-sensorised clothespin test.** The transracial amputee subject picking and placing non-
20
21 841 sensorised pins arranged in four triplets of different stiffness as previously reported (22). The amputee
22
23 842 controls prosthesis wrist pronation-supination and hand opening-closing simultaneously while generating
24
25 843 natural motions.

26
27 844
28
29 845 **Movie 3. Sensorised clothespin test.** The transracial amputee subject picking and placing sensorised pins of
30
31 846 different stiffness. The target force windows to successfully relocate each pin are 7-15% (yellow pin), 13-
32
33 847 23% (red pin), 23-32% (green pin), and 35-43% (black pin) of the prosthesis maximum force. The movie
34
35 848 shows the amputee's ability of fine controlling the prosthesis grip force while simultaneously controlling
36
37 849 hand rotation, while not triggering the light sensor.

38
39
40 850
41
42 851 **Movie 4. Block turn test.** The transradial amputee executes a block-turn task involving fine control of
43
44 852 prosthesis wrist pronation-supination and hand opening-closing simultaneously in the precise positioning of
45
46 853 a narrow wooden block in equilibrium on a wooden shelf.

47
48 854
49
50 855 **Movie 5. Egg manipulation.** The transradial amputee precisely controls hand opening-closing grip force for
51
52 856 grasping an egg. The movie shows the amputee's ability of fine grasping force control while rotating the
53
54 857 prosthetic wrist without breaking the egg.

55
56
57 858
58
59 859 **Movie 6. Cable induced movement artefacts.** How our proposed system being transparent to mechanically
60
860 induced cable-related movement artifacts visibly present in the recorded electromyograms. Despite the

1
2 861 artificially induced noise condition the prosthesis does not inadvertently activate unwanted degrees of
3
4 862 freedom. The movie also shows amputee's voluntary prosthesis control under noise condition.
5
6 863
7
8 864 **Movie 7. Manipulation of heavy objects.** Our proposed system enabling grasping and manipulating heavy
9
10 865 objects including a 1.5L water bottle, a task that would be challenging for state of the art non-invasive
11
12 866 myoelectric systems.
13
14
15
16
17
18
19
20
21
22
23
24
25
26
27
28
29
30
31
32
33
34
35
36
37
38
39
40
41
42
43
44
45
46
47
48
49
50
51
52
53
54
55
56
57
58
59
60